Cell Reports

Article

A Small-RNA-Mediated Feedback Loop Maintains Proper Levels of 22G-RNAs in *C. elegans*

Graphical Abstract

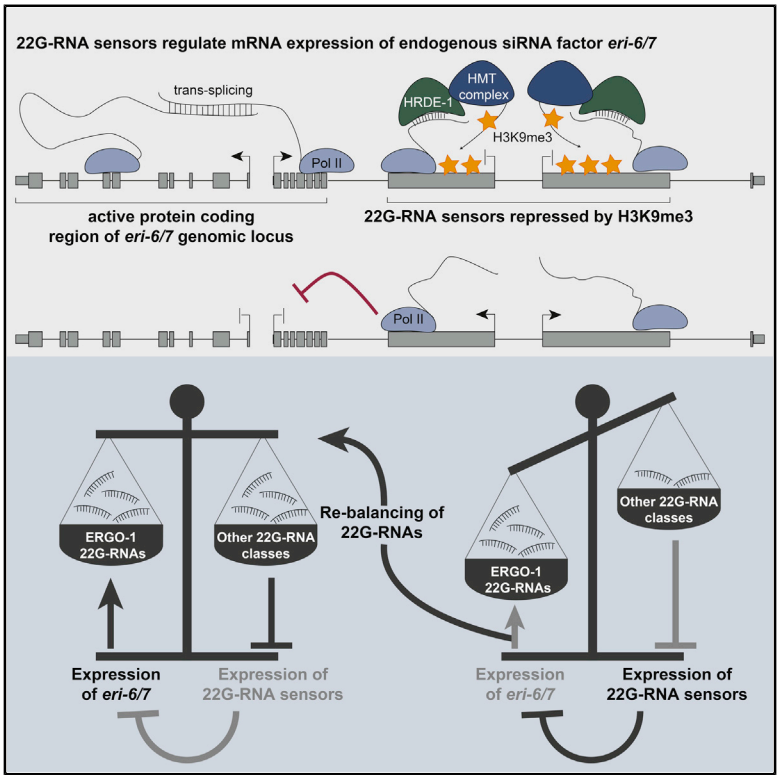

Highlights

- The *eri-6/7* genomic locus harbors two regions targeted by MUT-16-dependent 22G-RNAs
- Loss of these 22G-RNAs disrupts expression of *eri-6/7* mRNA and thus ERGO-1 26G-RNAs
- Modulation of ERGO-1 26G-RNA biogenesis tunes MUT-16-dependent 22G-RNAs production
- This pathway acts like a feedback loop to ensure homeostasis of 22G-RNA production

Authors

Alicia K. Rogers, Carolyn M. Phillips

Correspondence

cphil@usc.edu

In Brief

Rogers and Phillips identify a small-RNA-mediated feedback mechanism that regulates the expression of endogenous siRNAs. By modulating the expression of the endogenous siRNA biogenesis factor ERI-6/7, this feedback mechanism ensures homeostasis of small RNA production and ultimately mRNA expression.

Rogers & Phillips, 2020, Cell Reports *33*, 108279
October 20, 2020
https://doi.org/10.1016/j.celrep.2020.108279

CellPress

Cell Reports

CellPress
OPEN ACCESS

Article

A Small-RNA-Mediated Feedback Loop Maintains Proper Levels of 22G-RNAs in *C. elegans*

Alicia K. Rogers[1] and Carolyn M. Phillips[1,2,*]
[1]Department of Biological Sciences, University of Southern California, Los Angeles, CA 90089, USA
[2]Lead Contact
*Correspondence: cphil@usc.edu
https://doi.org/10.1016/j.celrep.2020.108279

SUMMARY

RNA interference (RNAi) is an essential regulatory mechanism in all animals. In *Caenorhabditis elegans*, several classes of small RNAs act to silence or license expression of mRNA targets. ERI-6/7 is required for the production of some endogenous small interfering RNAs (siRNAs) and acts as a negative regulator of the exogenous RNAi pathway. We find that the genomic locus encoding *eri-6/7* contains two distinct regions that are targeted by endogenous siRNAs. Loss of these siRNAs disrupts *eri-6/7* mRNA expression, resulting in increased production of siRNAs from other small RNA pathways because these pathways compete with *eri-6/7*-dependent transcripts for access to the downstream siRNA amplification machinery. Thus, the pathway acts like a small-RNA-mediated feedback loop to ensure homeostasis of gene expression by small RNA pathways. Similar feedback loops that maintain chromatin homeostasis have been identified in yeast and *Drosophila melanogaster*, suggesting an evolutionary conservation of feedback mechanisms in gene regulatory pathways.

INTRODUCTION

The evolutionarily conserved RNA interference (RNAi) pathways in metazoans are essential for the proper regulation of endogenous and exogenous gene expression. Argonaute proteins and their associated small RNAs are integral components of RNA-induced silencing complexes (RISCs), which transcriptionally and post-transcriptionally regulate target transcripts (Buckley et al., 2012; Burkhart et al., 2011; Claycomb, 2014; Gu et al., 2012; Guang et al., 2008, 2010; Hutvagner and Simard, 2008). Several mechanisms exist to generate the small RNA guides within RISC, each with distinct features. For instance, the RNase-III-like enzyme Dicer generates small interfering RNAs (siRNAs) by cleaving exogenous and endogenous long double-stranded RNAs (dsRNAs) (Bernstein et al., 2001; Ketting et al., 2001). In *Caenorhabditis elegans*, these siRNAs initiate amplification of additional secondary siRNAs within a perinuclear granule referred to as the *Mutator* focus (Gent et al., 2010; Gu et al., 2009; Pak and Fire, 2007; Phillips et al., 2012; Sijen et al., 2007; Vasale et al., 2010). MUT-16 is required to assemble the *mutator* complex, which includes an RNA-dependent RNA polymerase (RdRP) that is responsible for the amplification of 22G-RNAs (Phillips et al., 2012; Zhang et al., 2011). Secondary siRNAs dependent on the *mutator* complex are essential for robust RISC-mediated silencing (Gent et al., 2010; Ghildiyal and Zamore, 2009; Gu et al., 2009; Lee and Collins, 2007; Pak and Fire, 2007; Sijen et al., 2007; Vasale et al., 2010). RISC-meditated regulation is responsible for maintaining homeostasis, appropriate gene expression, and silencing of foreign genetic elements, by either post-transcriptionally regulating targets in the cytoplasm or transcriptionally regulating mRNAs at the chromatin level by directing the establishment of the repressive chromatin mark H3K9me3 (Buckley et al., 2012; Burkhart et al., 2011; Castel and Martienssen, 2013; Claycomb, 2014; Guang et al., 2008, 2010; Ketting, 2011).

ERI-6/7 is an RNA helicase that is required for the biogenesis of ERGO-1-class 26G-RNAs in embryos and thus is necessary to target complementary transcripts to the *mutator* complex for the production of high levels of 22G-RNAs in adults (Figure S1; Fischer et al., 2011). In *C. elegans*, the *eri-6/7* transcript is produced by a *trans*-splicing event between the *eri-6* and *eri-7* pre-messenger RNAs (pre-mRNAs) (Fischer et al., 2008). If the function of ERI-6/7 is disrupted, animals display an enhanced RNAi (Eri) phenotype (Fischer et al., 2008, 2011). It has been proposed that this Eri phenotype stems from a requirement by both the ERGO-1 26G-RNA pathway and the RDE-1 exogenous siRNA pathway for the shared downstream use of the *mutator* complex for siRNA amplification (Duchaine et al., 2006; Lee et al., 2006).

The genomic locus of *eri-6* contains several annotated isoforms. Four of the isoforms (*eri-6[a–d]*) encode the *eri-6* sequence that corresponds to the functional *eri-6/7* protein, whereas the remaining annotated isoforms (*eri-6[e–f],* formerly annotated as T01A4.3) do not contain a sequence that encodes the ERI-6/7 protein. Nested within the *eri-6* genomic locus is the intronless gene C41D11.6, whose function has not previously

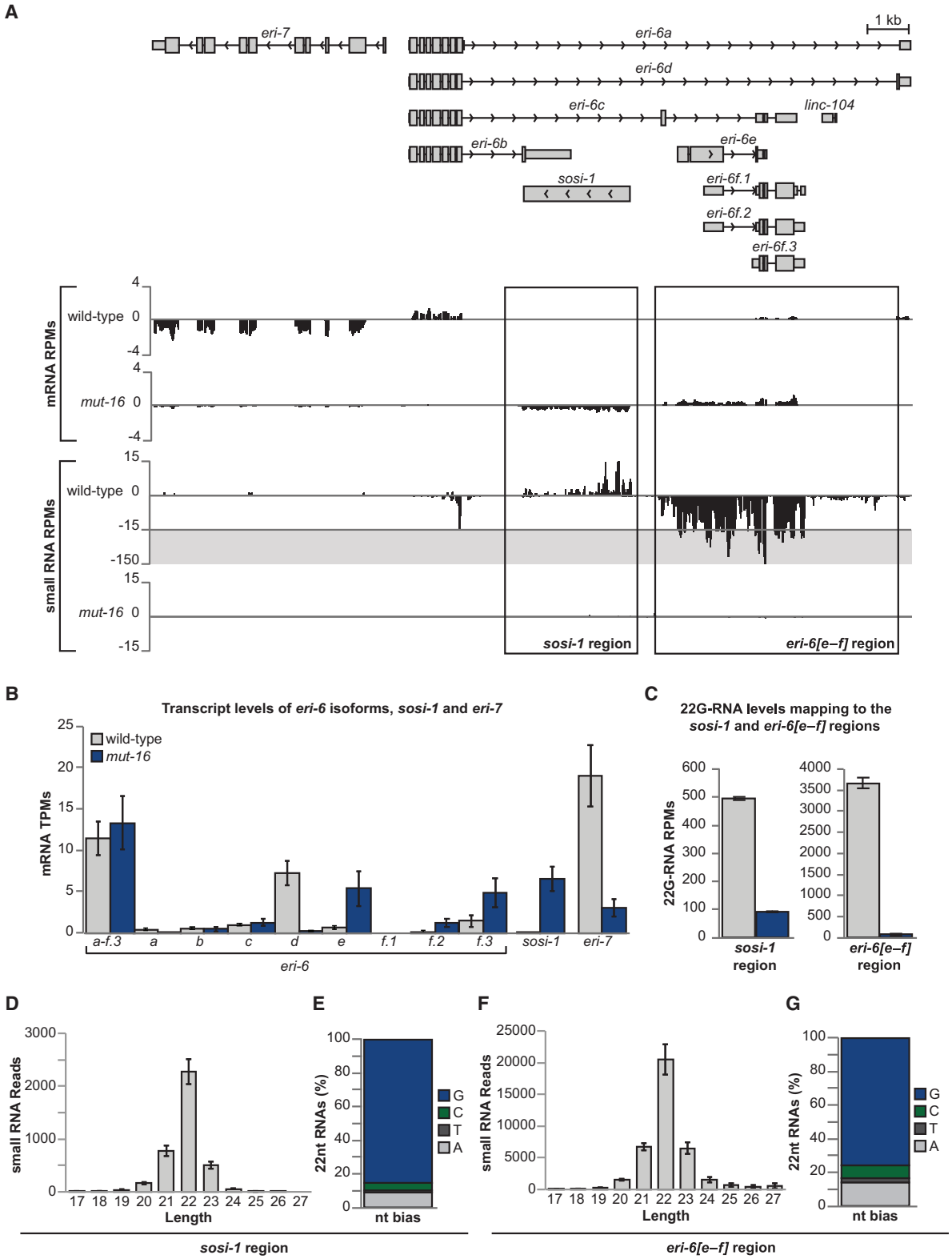

Figure 1. *eri-6/7* Expression Is Altered in *mut-16* Mutants

(A) mRNA and small RNA reads per million (RPMs) across the *eri-7* and *eri-6* genomic locus in wild-type and *mut-16* mutant animals. The *sosi-1* and *eri-6[e–f]* regions are boxed.

(legend continued on next page)

been described. Based on our findings described in this work, we have named C41D11.6 *sosi-1* (*sensor of siRNAs-1*). Transcriptional silencing of *sosi-1* is mediated by the nuclear Argonaute protein HRDE-1 in the *C. elegans* germline by deposition of the repressive chromatin mark H3K9 trimethylation (H3K9me3) (Ni et al., 2014). In *hrde-1* mutants, which are incapable of mediating H3K9me3 deposition at germline nuclear RNAi target loci, H3K9me3 and small RNAs are lost at the *sosi-1* locus, which corresponds to increased *sosi-1* mRNA expression (Ni et al., 2014).

It has been observed that in *mut-16* mutant embryos, which are incapable of synthesizing 22G-RNAs complementary to mRNA targets of multiple small RNA pathways, ERGO-1-class 26G-RNAs are strongly depleted relative to wild-type embryos (Zhang et al., 2011). This finding is surprising, as it is generally thought that MUT-16 acts only in the secondary siRNA pathway, placing it functionally downstream of ERI-6/7 and ERGO-1 (Figure S1). Here, we show that the *eri-6* genomic locus contains two regions that are targeted in a MUT-16-dependent manner by 22G-RNAs—the *eri-6* isoforms, *eri-6[e–f]*, and *sosi-1*. Loss of 22G-RNAs targeting these regions results in reduced expression of the *eri-6/7 trans*-spliced mRNA and loss of ERGO-1-class 26G-RNAs. We propose that these regions act independently of one another as sensors for HRDE-1-loaded MUT-16-dependent 22G-RNA levels to regulate ERI-6/7 function, which ultimately feeds back to regulate the biogenesis of 22G-RNAs associated with other small RNA pathways. Thus, these results reveal the existence of a regulatory network that modulates the expression of the exogenous and endogenous RNAi pathways by targeting sensors contained within the *eri-6* gene locus. Furthermore, this regulatory network explains the depletion of 26G-RNAs in *mut-16* mutants, despite the well-documented role of MUT-16 in siRNA amplification downstream of 26G-RNA biogenesis.

RESULTS

eri-6/7 Expression Is Reduced in *mut-16* Mutants

MUT-16 is a core component of the small RNA amplification complex that is responsible for synthesis of 22G-RNAs within the *Mutator* focus (Phillips et al., 2012; Zhang et al., 2011). Previously, we generated mRNA sequencing (mRNA-seq) and small RNA-seq libraries from synchronized day 1 adult wild-type and *mut-16* mutant animals grown at 20°C (Rogers and Phillips, 2020). Interestingly, we noticed significant differential expression of the *eri-6/7* locus in *mut-16* mutants compared with wild-type animals (Figures 1A and 1B). The *eri-6/7* transcript is produced by a *trans*-splicing event of separate *eri-6* and *eri-7* pre-mRNAs (Fischer et al., 2008). The *eri-6* locus contains the protein-coding isoforms (*eri-6[a–d]*) and other annotated isoforms (*eri-6[e–f]*) that do not encode an *eri-6* pre-mRNA that can be *trans*-spliced to form *eri-6/7*. In wild-type animals, *eri-6d*, which is the primary protein-coding isoform, is the most highly expressed *eri-6* isoform; however, in *mut-16* mutants the expression of the *eri-6d* isoform is reduced significantly, and instead, the *eri-6e* and *eri-6f* isoforms are predominantly expressed (Figures 1A and 1B). The *eri-7* locus also exhibited significantly reduced transcript levels in *mut-16* mutants compared with those of wild-type animals (Figures 1A and 1B). Furthermore, in *mut-16* mutants, we observed a significant increase in the expression of the *sosi-1* gene, which is found in an intron of *eri-6* (Figures 1A and 1B). These results indicate that in *mut-16* mutants, the expression of both *sosi-1* and *eri-7* are altered, and there is a change in the selection of isoforms from the *eri-6* genomic locus.

To determine whether the observed differential expression of the *eri-6* and *eri-7* pre-mRNAs correlated with changes in small RNAs, we compared small RNA-seq libraries generated from wild-type and *mut-16* mutants. In wild-type animals, we observed high levels of small RNA reads mapping to the genomic locus of *sosi-1* (genomic coordinates I:4459750-4462935, which we call the *sosi-1* region) and to the *eri-6[e–f]* isoforms of *eri-6* (genomic coordinates I:4463370-4469204, which we call the *eri-6[e–f]* region) (Figures 1A and 1C). In contrast, small RNAs mapping to the *sosi-1* region and *eri-6[e–f]* region are depleted in *mut-16* mutants (Figures 1A and 1C). Further analysis revealed the small RNAs mapping to the *sosi-1* region and *eri-6[e–f]* region are predominantly 22G-RNAs, which is not surprising due to their dependence on MUT-16 (Figures 1D–1G). It should be noted that the *eri-6f* portion of the *eri-6[e–f]* region is 97.3% identical to the uncharacterized intronless gene K09B11.4, which is a 22G-RNA target situated near a Piwi-interacting RNA (piRNA) cluster (Figure S2). The proximity of K09B11.4 to a piRNA cluster (Ruby cluster genomic coordinates IV:13.5M-17.2M) is intriguing; however, further experiments will need to be performed to determine whether the *eri-6[e–f]* region or K09B11.4 are the source of the 22G-RNAs. Therefore, our data reveal that *mutator*-complex-dependent 22G-RNAs targeting *sosi-1* and the *eri-6* isoforms *eri-6[e–f]* are lost in *mut-16* mutants, which correlates with the upregulation of *sosi-1* and *eri-6[e–f]* mRNA and downregulation of the protein-coding regions of *eri-6 (eri-6d)* and *eri-7* pre-mRNAs.

The *sosi-1* and *eri-6[e–f]* Regions Are Targeted by HRDE-1-Loaded MUT-16-Dependent 22G-RNAs

Secondary WAGO-class 22G-RNAs, which require the *mutator* complex for their biogenesis, can be dependent on upstream

(B) Shown are transcripts per kilobase million (TPMs) for *eri-6* isoforms, *sosi-1*, and *eri-7* in wild-type and *mut-16* mutant mRNA-seq libraries. Error bars indicate standard deviation. n = 3 biological replicates.
(C) Shown are 22G-RNA levels in RPMs mapping to the *sosi-1* and *eri-6[e–f]* regions in small RNA libraries from wild-type animals and *mut-16* mutants. Error bars indicate standard deviation. n = 3 biological replicates.
(D) Shown are size profiles of all reads mapping to the *sosi-1* region in wild-type small RNA libraries. Error bars indicate standard deviation between replicates. n = 3 biological replicates.
(E) Shown is the nucleotide represented in the first position of 22-nucleotide (nt) reads mapping to the *sosi-1* region in wild-type small RNA libraries.
(F) Shown are size profiles of all reads mapping to the *eri-6[e–f]* region in wild-type small RNA libraries. Error bars indicate standard deviation between replicates. n = 3 biological replicates.
(G) Shown is the nucleotide represented in the first position of 22-nt reads mapping to the *eri-6[e–f]* region in wild-type small RNA libraries. See also Figures S1 and S2.

primary small RNA pathways including piRNAs, also referred to as 21U-RNAs in *C. elegans,* and ERGO-1-class 26G-RNAs (Phillips et al., 2012; Zhang et al., 2011). To determine whether the 22G-RNAs targeting the *sosi-1* region and *eri-6[e–f]* region are dependent on piRNAs or ERGO-1-class 26G-RNAs, we generated small RNA libraries from *prg-1*, *ergo-1*, and *prg-1; ergo-1* double mutants, respectively. Previously, it was shown that piRNA-initiated silencing can be maintained independent of PRG-1 through the activity of the *mutator* complex and the Argonaute protein HRDE-1 (Ashe et al., 2012; Luteijn et al., 2012; Shirayama et al., 2012). To ensure we effectively disrupted all piRNA-initiated gene silencing, we also generated small RNA libraries from *prg-1; hrde-1* double mutants. We assessed 22G-RNA levels mapping to the *sosi-1* region and *eri-6[e–f]* region in *mut-16*, *prg-1*, and *ergo-1* single mutants and in *prg-1; ergo-1* and *prg-1; hrde-1* double mutants compared with those of wild-type animals. We found that 22G-RNA levels mapping to the *sosi-1* region are not significantly changed in *ergo-1* mutants and are slightly upregulated in *prg-1* and *prg-1; ergo-1* mutants (Figure 2A). However, 22G-RNA levels mapping to the *sosi-1* region are significantly reduced in *prg-1; hrde-1* mutants (Figures 2A and 2B). Similar results were observed previously in *hrde-1* single mutants (Ni et al., 2014). Using piRTarBase, a database that curates both predicted and experimentally identified piRNA target sites, we found that the mRNA sequence of *sosi-1* harbors 12 sequence-predicted piRNA-binding sites (Wu et al., 2019; Zhang et al., 2018), suggesting that the MUT-16-dependent and HRDE-1-loaded 22G-RNAs mapping to the *sosi-1* region may be initiated by piRNAs.

Levels of 22G-RNAs mapping to the *eri-6[e–f]* region are moderately, but significantly, reduced in both *ergo-1* and *prg-1* single mutants and were more strongly reduced in *prg-1; hrde-1* double mutants (Figures 2A and 2B). Surprisingly, 22G-RNA levels targeting the *eri-6[e–f]* region were not affected in *prg-1; ergo-1* double mutants (Figure 2A); however, these libraries are depleted for two major classes of 22G-RNAs that may result in increased sampling of other 22G-RNA classes. Thus, another class of 22G-RNAs targeting the *eri-6[e–f]* region may be overrepresented in the *prg-1; ergo-1* mutant libraries. Because *hrde-1* mutants were previously shown to exhibit reduced small RNA levels mapping to the *eri-6[e–f]* region (Ni et al., 2014), we were unable to definitively conclude whether the HRDE-1-loaded 22G-RNAs are piRNA initiated. However, using piRTarBase, we found both sequence-predicted and cross-linking, ligation, and sequencing of hybrids (CLASH)-identified piRNA-binding sites within the mRNA sequences of *eri-6[e–f]* (25 sequence predicted, 14 CLASH identified) and its paralog K09B11.4 (6 sequence predicted, 6 CLASH identified) (Shen et al., 2018; Wu et al., 2019; Zhang et al., 2018), suggesting the HRDE-1-loaded 22G-RNAs may be piRNA initiated. The piRNAs identified as binding to K09B11.4 were also found to bind *eri-6f* transcripts (Shen et al., 2018). Overall, these data suggest that the MUT-16-dependent 22G-RNAs that map to the *eri-6[e–f]* region may include ERGO-1-dependent 22G-RNAs, piRNA-dependent 22G-RNAs, HRDE-1-loaded 22G-RNAs, and potentially other 22G-RNA classes.

Next, to determine whether ERGO-1-dependent 22G-RNAs or piRNA-dependent 22G-RNAs affect the expression of *sosi-1* or *eri-6[e–f]* transcripts, we performed qRT-PCR using cDNA generated from wild-type animals, *mut-16* mutants, *ergo-1* mutants, and *prg-1* mutants with primers targeting *sosi-1* and *eri-6e* transcripts. We designed our qPCR primers to detect the expression of the *eri-6e* transcript to prevent detecting the expression of the K09B11.4 transcript, which is highly similar to *eri-6f*. It should be noted that *sosi-1* and *eri-6e* are expressed at very low levels in wild-type animals, and therefore, only increased expression can be accurately assessed. We found that, compared to wild-type animals, expression of *sosi-1* is significantly upregulated in *mut-16* mutants and is slightly upregulated in *prg-1* mutants but is not upregulated in *ergo-1* mutants (Figure 2C). Expression of *eri-6e* is significantly upregulated in *mut-16* mutants but is not upregulated in *ergo-1* or *prg-1* mutants (Figure 2C). Thus, our qRT-PCR results corroborate our mRNA-seq results demonstrating that *sosi-1* and *eri-6e* expression is significantly upregulated in *mut-16* mutants (Figures 1A, 2B, and 2C). Next, we generated mRNA-seq libraries generated from *prg-1; hrde-1* and *prg-1; ergo-1* libraries and assessed the expression levels of *sosi-1* and *eri-6e*. We observed that, compared to wild-type animals, *prg-1; ergo-1* mutants did not exhibit changes in the expression levels of *sosi-1* or *eri-6e* (Figure 2D). In contrast, *prg-1; hrde-1* mutants had increased levels of expression of both *sosi-1* and *eri-6e*, compared to wild-type animals (Figures 2B and 2D). Similar results were observed previously in *hrde-1* single mutants (Ni et al., 2014), indicating that HRDE-1 is essential for maintaining the repression of both *sosi-1* and *eri-6e* in wild-type animals. Taken together, our small RNA-seq and mRNA-seq data suggest that *sosi-1* and *eri-6[e–f]* are targeted predominately by HRDE-1-loaded 22G-RNAs.

sosi-1 and *eri-6[e–f]* Regions Are Independently Regulated by MUT-16-Dependent 22G-RNAs

To address whether the small RNAs mapping to the *sosi-1* region, *eri-6[e–f]* region, or both regions combined were directly responsible for the regulation of *eri-6/7*, we generated *C. elegans* strains that lacked either the *sosi-1* region (*sosi-1Δ(cmp262)*), the *eri-6[e–f]* region (*eri-6[e–f]Δ(cmp261)*), or both regions (*sosi-1 eri-6[e–f]Δ(cmp263)*) in wild-type and *mut-16* mutants (Figure 3A). First, we assessed how expression of the *sosi-1* and *eri-6e* transcript levels are affected in our mutants using qRT-PCR and mRNA-seq. Compared to wild-type animals, only *eri-6[e–f]Δ mut-16* double mutants exhibited upregulated *sosi-1* expression, which was similar to the *mut-16* mutant alone (Figures 3B and S3). Both *sosi-1Δ* and *sosi-1 eri-6[e–f]Δ*, with and without the *mut-16* mutant, did not exhibit upregulated *sosi-1* expression, as expected, because the *sosi-1* locus is deleted in these strains (Figures 3B and S3). Similarly, *eri-6e* expression is significantly upregulated only in *sosi-1Δ mut-16* double mutants, similar to the *mut-16* mutant alone (Figures 3B and S3). *sosi-1Δ* mutants expressed *eri-6e* transcripts at levels similar to those of wild-type animals, and both *eri-6[e–f]Δ* and *sosi-1 eri-6[e–f]Δ*, lacking the *eri-6e* locus, either in the presence or absence of the *mut-16* mutant, displayed severely reduced expression of *eri-6e* transcripts (Figures 3B and S3). In addition, we generated small RNA-seq libraries from *sosi-1Δ*, *eri-6[e–f]Δ*, and *sosi-1 eri-6[e–f]Δ* mutants in wild-type and *mut-16* backgrounds and found that the 22G-RNAs mapping to the *sosi-1* region were not

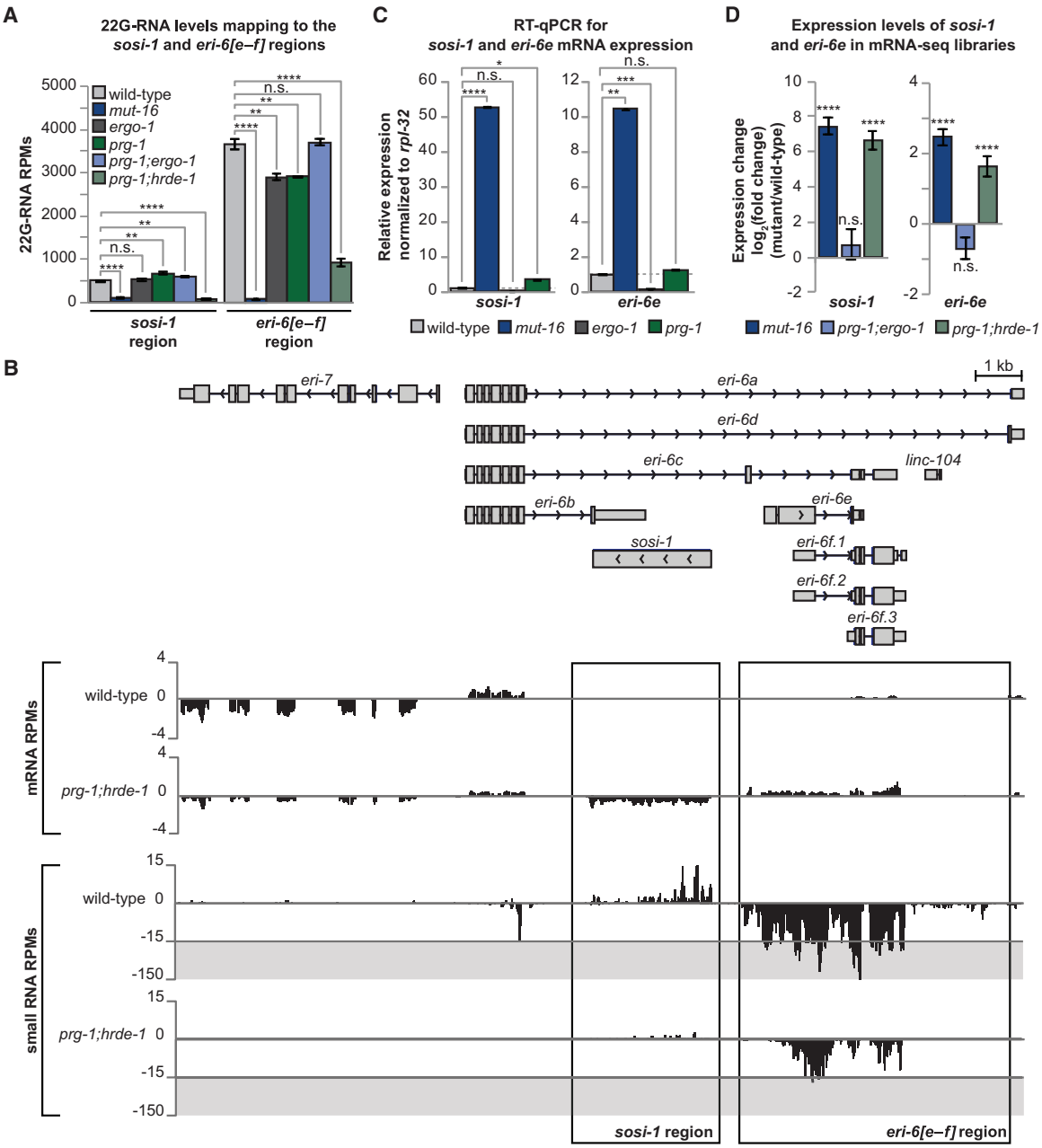

Figure 2. The *sosi-1* and *eri-6[e–f]* Regions Are Targeted by HRDE-1-Loaded MUT-16-Dependent 22G-RNAs

(A) Shown are 22G-RNA levels in RPMs mapping to the *sosi-1* and *eri-6[e–f]* regions in small RNA libraries from wild-type animals, *mut-16* mutants, *ergo-1* mutants, *prg-1* mutants, *prg-1; ergo-1* mutants, and *prg-1; hrde-1* mutants. Error bars represent standard deviation. n = 3 biological replicates.

(B) mRNA and small RNA RPMs across the *eri-7* and *eri-6* genomic locus in wild-type and *prg-1; hrde-1* mutant animals. The *sosi-1* and *eri-6[e–f]* regions are boxed.

(C) qRT-PCR assay of *sosi-1* and *eri-6e* expression in *mut-16* mutants, *ergo-1* mutants, and *prg-1* mutants normalized to expression in wild-type animals. Error bars represent standard deviation. Dashed line represents 1. n = 3 biological replicates.

(D) Shown is the the $\log_2$(fold change) of *sosi-1* and *eri-6e* transcript levels in mRNA-seq libraries of *mut-16* mutants, *prg-1; ergo-1* mutants, and *prg-1; hrde-1* mutants compared to those of wild-type animals. Error bars represent $\log_2$(standard error). n = 3 biological replicates. n.s., not significant and indicates a $p > 0.05$; *$p \leq 0.05$; **$p \leq 0.01$; ***$p \leq 0.001$; ****$p \leq 0.0001$.

dependent on the existence of the *eri-6[e–f]* region and vice versa (Figure 3C). These data indicate that the *sosi-1* and *eri-6 [e–f]* regions are regulated independently of one another by MUT-16-dependent 22G-RNAs and that deletion of either region is not sufficient to prevent upregulation of the other region in a *mut-16* mutant.

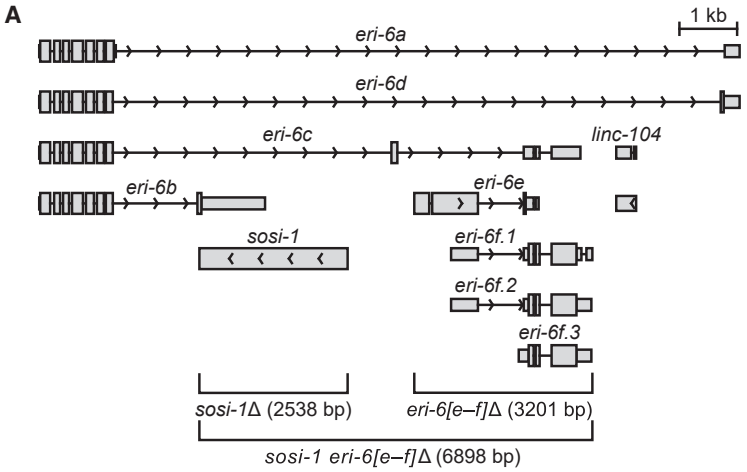

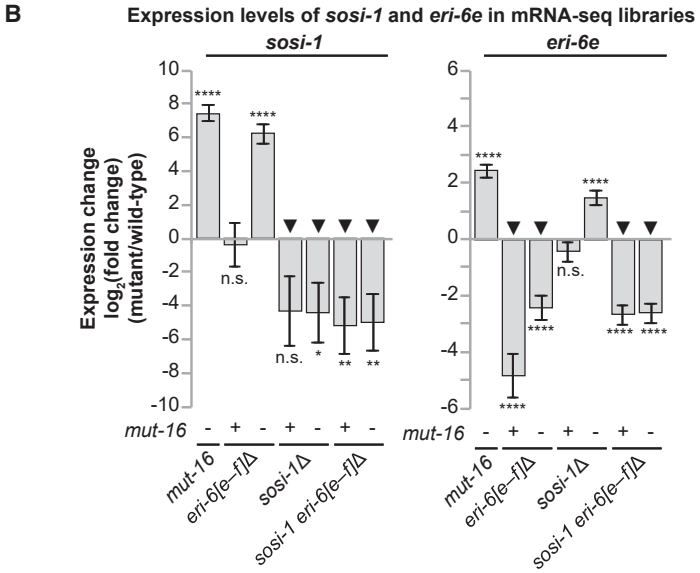

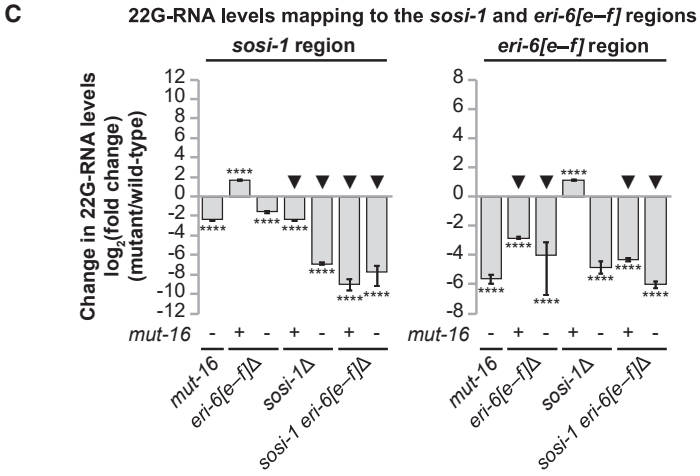

Figure 3. *sosi-1* and *eri-6[e–f]* Regions Are Independently Regulated

(A) Schema of transgenic *C. elegans* in which the *sosi-1* region (*sosi-1*Δ), *eri-6[e–f]* region (*eri-6[e–f]*Δ), or both regions (*sosi-1 eri-6[e–f]*Δ) are removed.

(B) The $\log_2$(fold change) of *sosi-1* and *eri-6e* transcript levels in mRNA-seq libraries of *mut-16* mutants, *eri-6[e–f]*Δ mutants, *eri-6[e–f]*Δ *mut-16* mutants, *sosi-1*Δ mutants, *sosi-1*Δ *mut-16* mutants, *sosi-1 eri-6[e–f]*Δ mutants, and *sosi-1 eri-6[e–f]*Δ *mut-16* mutants compared to wild-type animals. Error bars represent $\log_2$(standard error). n = 3 biological replicates. Black triangles denote mutants in which the region assayed is deleted.

(C) The $\log_2$(fold change) of 22G-RNAs mapping to the *sosi-1* region and *eri-6[e–f]* region in small RNA libraries generated from wild-type animals, *mut-16* mutants, *eri-6[e–f]*Δ mutants, *eri-6[e–f]*Δ *mut-16* mutants, *sosi-1*Δ mutants, *sosi-1*Δ *mut-16* mutants, *sosi-1 eri-6[e–f]*Δ mutants, and *sosi-1 eri-6[e–f]*Δ *mut-16* mutants compared to wild-type animals. Error bars represent $\log_2$(standard error). n = 3 biological replicates. Black triangles denote mutants in which the region assayed is deleted. n.s., not significant and indicates a $p > 0.05$; *$p \leq 0.05$; **$p \leq 0.01$; ***$p \leq 0.001$; ****$p \leq 0.0001$. See also Figure S3.

A

Eri RNAi Assay

	dpy-13	lir-1
wild-type	+	-
mut-16	-	-
ergo-1	+++	+++
eri-6[e–f]Δ	+	-
sosi-1Δ	+	-
sosi-1 eri-6[e–f]Δ	+	-
eri-6[e–f]Δ mut-16	-	-
sosi-1Δ mut-16	-	-
sosi-1 eri-6[e–f]Δ mut-16	-	-

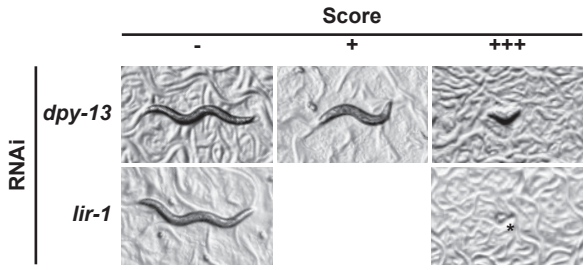

B

Taqman-qPCR for expression of ERGO-1 class 26G-RNAs

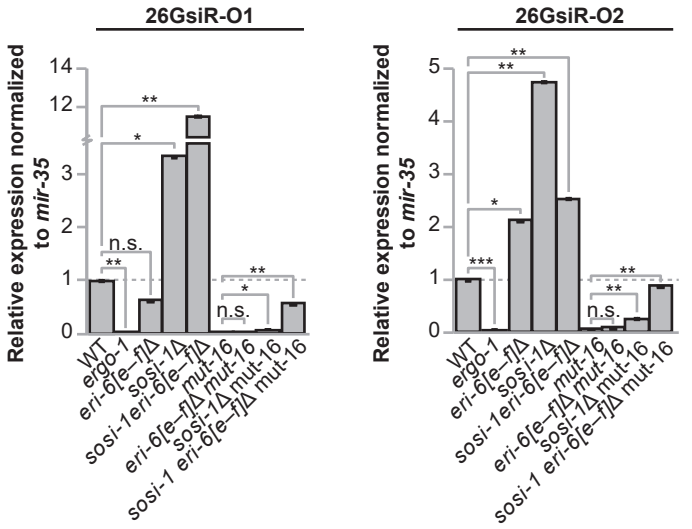

C

Taqman-qPCR for expression of 22GsiR-O1

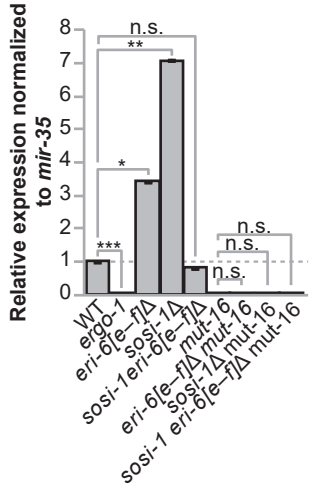

D

26G-RNAs mapping to ERGO-1 targets normalized to *mir-35* family mapping reads

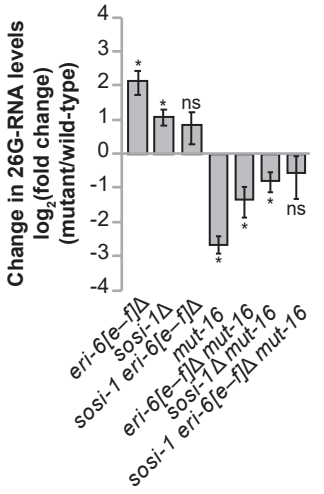

E

22G-RNAs mapping to ERGO-1 targets normalized to *mir-35* family mapping reads

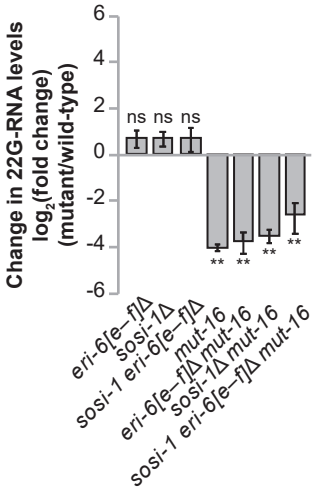

F

Expression levels of *eri-6/7* in mRNA-seq libraries

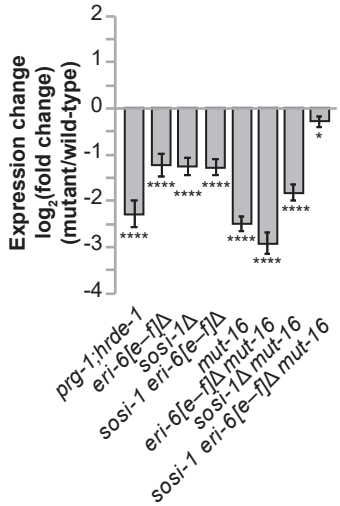

(legend on next page)

sosi-1 and *eri-6[e–f]* Regions Regulate ERI-6/7 Function and Expression

ERI-6/7 is required for the production of ERGO-1-class 26G-RNAs (Fischer et al., 2011). When ERI-6/7 function is disrupted, animals display an enhanced RNAi (Eri) phenotype (Fischer et al., 2008). To assess whether the *sosi-1*Δ, *eri-6[e–f]*Δ, or *sosi-1 eri-6[e–f]*Δ deletions affect ERI-6/7 function, we performed an RNAi feeding assay to determine whether the mutants exhibited wild-type, enhanced, or deficient RNAi capabilities. Enhanced RNAi capabilities can be assessed using *lir-1* and *dpy-13* RNAi. The first generation of Eri mutants exposed to *lir-1* RNAi exhibit lethality as a consequence of enhanced nuclear silencing of the *lir-1/lin-26* polycistronic pre-mRNA, whereas the first generation of wild-type animals exposed to *lir-1* RNAi do not exhibit a phenotype (Bosher et al., 1999; Guang et al., 2008; Figure 4A). Similarly, RNAi of the collagen gene *dpy-13* in wild-type animals results in only a modestly shorter animal, whereas RNAi of the same gene in Eri mutant animals causes a severe Dumpy (Dpy) phenotype, possibly due to knockdown of multiple paralogous collagen genes (Kennedy et al., 2004; Zhuang et al., 2013; Figure 4A). Therefore, we assayed the RNAi competency of each deletion, with and without the *mut-16* mutation, compared to our control strains (wild-type [RNAi competent], *mut-16* [RNAi deficient], and *ergo-1* [enhanced RNAi]) following exposure to *dpy-13*, *lir-1,* or a control RNAi clone (L4440). The effects of the RNAi clones were scored based on whether the strains exhibited no phenotype (−), a weak phenotype (+), or a strong phenotype (+++) (Figure 4A). We observed that the *sosi-1*Δ, *eri-6[e–f]*Δ, and *sosi-1 eri-6[e–f]*Δ deletion mutants exhibited wild-type RNAi competency for both *dpy-13* and *lir-1* RNAi (Figure 4A). As expected, all strains carrying the *mut-16* mutant, which is required for response to exogenous dsRNA, were RNAi defective for *dpy-13* RNAi (Figure 4A). RNAi of *lir-1* does not elicit a phenotype in wild-type animals until the second generation of exposure; therefore, after a single generation of *lir-1* RNAi, we did not observe a phenotypic difference between wild-type and *mut-16* mutants (Figure 4A). These data indicate that the three deletions do not affect the function of the ERI-6/7 protein.

Because we could not assess the function of ERI-6/7 in the *mut-16* mutants using the Eri RNAi assay, in parallel, we directly assessed the ability of each strain to generate ERGO-1-class 26G-RNAs using TaqMan qRT-PCR from embryos. We quantified the levels of two ERGO-1-class 26G-RNAs, 26G-siR-O1 and 26G-siR-O2, derived from the C40A11.10 and E01G4.7 loci, respectively. In addition, we quantified the levels of the 22G-RNAs generated downstream of 26G-siR-O1 (22G-siR-O1). As previously observed, 26G-siR-O1 and 26G-siR-O2 levels, as well as 22G-siR-O1 levels, were strongly depleted in embryos of *ergo-1* and *mut-16* mutants compared to those in wild-type embryos (Figures 4B and 4C; Fischer et al., 2011; Zhang et al., 2011). Consistent with the results of our RNAi assay, *sosi-1*Δ, *eri-6[e–f]*Δ, and *sosi-1 eri-6[e–f]*Δ mutants maintained the ability to generate ERGO-1-class 26G-RNAs and their downstream 22G-RNAs for 26G-siR-O1 and 26G-siR-O2, at levels comparable to or higher than in wild-type embryos (Figures 4B and 4C).These data further support that these deletions do not affect ERI-6/7 function. 26G-siR-O1, 26GsiR-O2, and 22G-siR-O1 levels were strongly depleted in *sosi-1*Δ *mut-16* mutants and *eri-6[e–f]*Δ *mut-16* mutants (Figures 4B and 4C). In contrast, the *sosi-1 eri-6[e–f]*Δ *mut-16* mutant was able to produce 26G-siR-O1 and 26G-siR-O2, but not 22G-siR-O1, at levels comparable to wild-type embryos and significantly higher than *mut-16* mutants alone (Figures 4B and 4C), which indicates that ERI-6/7 function is restored in this strain. Furthermore, an analysis of the levels of all 26G-RNAs and 22G-RNAs mapping to ERGO-1 class targets relative to the small RNAs mapping to members of the germline-specific *mir-35* family (*mir-35–42*), which are not amplified by the *mutator* complex, indicated that, compared to wild-type animals, the *sosi-1*Δ, *eri-6[e–f]*Δ, and *sosi-1 eri-6[e–f]*Δ mutants did not have reduced levels of 26G-RNAs or 22G-RNAs mapping to ERGO-1 class targets (Figures 4D and 4E). In fact, *sosi-1*Δ and *eri-6[e–f]*Δ single mutants produce significantly more ERGO-1-class 26G-RNAs than wild-type animals, although this increase in 26G-RNAs did not lead to a corresponding increase in ERGO-1-dependent 22G-RNAs, and the explanation for this increase in 26G-RNA levels

Figure 4. *sosi-1* and *eri-6[e–f]* Regions Regulate ERI-6/7 Function and Expression

(A) Sensitivity of wild-type animals, *ergo-1* mutants, *mut-16* mutants, *eri-6[e–f]*Δ mutants, *eri-6[e–f]*Δ *mut-16* mutants, *sosi-1*Δ mutants, *sosi-1*Δ *mut-16* mutants, *sosi-1 eri-6[e–f]*Δ mutants, and *sosi-1 eri-6[e–f]*Δ *mut-16* mutants to dsRNA clones—L4440 (control RNAi), *dpy-13,* or *lir-1*. Animals were scored as follows—for *dpy-13* RNAi: −, no phenotype; +, weak phenotype (slightly Dumpy); and +++, strong phenotype (severely Dumpy); and for *lir-1* RNAi: −, no phenotype; and +++, strong phenotype (lethal). For each strain, n = 120 individuals for each RNAi clone. Shown are representative images for the phenotypes scored in the Eri RNAi Assay of plated L1 animals after exposure for 3 days. *, dead larva.

(B) TaqMan qPCR assay for 26GsiR-O1 and 26GsiR-O2 levels in embryos of *ergo-1* mutants, *mut-16* mutants, *eri-6[e–f]*Δ mutants, *eri-6[e–f]*Δ *mut-16* mutants, *sosi-1*Δ mutants, *sosi-1*Δ *mut-16* mutants, *sosi-1 eri-6[e–f]*Δ mutants, and *sosi-1 eri-6[e–f]*Δ *mut-16* mutants normalized to *mir-35* expression and graphed relative to wild-type. Error bars represent standard deviation. Dashed line represents 1. n = 3 biological replicates.

(C) TaqMan qPCR assay for 22GsiR-O1 levels in embryos of *ergo-1* mutants, *mut-16* mutants, *eri-6[e–f]*Δ mutants, *eri-6[e–f]*Δ *mut-16* mutants, *sosi-1*Δ mutants, *sosi-1*Δ *mut-16* mutants, *sosi-1 eri-6[e–f]*Δ mutants, and *sosi-1 eri-6[e–f]*Δ *mut-16* mutants normalized to *mir-35* expression and graphed relative to wild-type. Error bars represent standard deviation. Dashed line represents 1. n = 3 biological replicates.

(D) The $\log_2$(fold change) of 26G-RNAs mapping to ERGO-1 targets in *mut-16* mutants, *eri-6[e–f]*Δ mutants, *eri-6[e–f]*Δ *mut-16* mutants, *sosi-1*Δ mutants, *sosi-1*Δ *mut-16* mutants, *sosi-1 eri-6[e–f]*Δ mutants, and *sosi-1 eri-6[e–f]*Δ *mut-16* mutants compared to wild-type animals. 26G-RNAs mapping to ERGO-1 targets are normalized to all reads mapping to *mir-35* family members (*mir-35–42*). Error bars represent $\log_2$(standard error). n = 3 biological replicates.

(E) The $\log_2$(fold change) of 22G-RNAs mapping to ERGO-1 targets in *mut-16* mutants, *eri-6[e-f]*Δ mutants, *eri-6[e–f]*Δ *mut-16* mutants, *sosi-1*Δ mutants, *sosi-1*Δ *mut-16* mutants, *sosi-1 eri-6[e–f]*Δ mutants, and *sosi-1 eri-6[e–f]*Δ *mut-16* mutants compared to wild-type animals. 22G-RNAs mapping to ERGO-1 targets are normalized to all reads mapping to *mir-35* family members (*mir-35–42*). Error bars represent $\log_2$(standard error). n = 3 biological replicates.

(F) The $\log_2$(fold change) of the *eri-6/7* transcript levels in mRNA-seq libraries of *prg-1; hrde-1* mutants, *mut-16* mutants, *eri-6[e–f]*Δ mutants, *eri-6[e–f]*Δ *mut-16* mutants, *sosi-1*Δ mutants, *sosi-1*Δ *mut-16* mutants, *sosi-1 eri-6[e–f]*Δ mutants, and *sosi-1 eri-6[e–f]*Δ *mut-16* mutants compared to wild-type animals. Error bars represent $\log_2$(standard error). n = 3 biological replicates. n.s., not significant and indicates a $p > 0.05$; *$p \leq 0.05$; **$p \leq 0.01$; ***$p \leq 0.001$; ****$p \leq 0.0001$.

is unknown (Figures 4D and 4E). In contrast, *sosi-1*Δ *mut-16*, *eri-6[e–f]*Δ *mut-16*, and *sosi-1 eri-6[e–f]*Δ *mut-16* mutants had reduced levels of 22G-RNAs mapping to ERGO-1 class targets due to the loss of the MUT-16 function (Figures 4D and 4E). Similar to our Taqman qPCR results, *sosi-1*Δ *mut-16* and *eri-6 [e–f]*Δ *mut-16* mutants had reduced levels of 26G-RNAs mapping to ERGO-1 class targets, whereas the *sosi-1 eri-6[e–f]*Δ *mut-16* mutant was able to produce 26G-RNAs, but not 22G-RNAs, mapping to ERGO-1 class targets at levels comparable to wild-type embryos and significantly higher than *mut-16* mutants alone (Figures 4D and 4E). Taken together, with the RNAi assay, these data further indicate that the three deletions do not affect the function of the ERI-6/7 protein.

Next, we sought to determine whether the *sosi-1*Δ, *eri-6[e–f]*Δ, or *sosi-1 eri-6[e–f]*Δ deletions affect *eri6/7* transcript levels. We assessed the expression of the *eri-6/7* transcript by measuring the expression levels of *eri6[a–d]* and *eri-7* in our mRNA-seq libraries generated from wild-type animals, *prg-1; hrde-1* mutants, *mut-16* mutants, and *sosi-1*Δ, *eri-6[e–f]*Δ, and *sosi-1 eri-6[e–f]*Δ mutants in both the wild-type and *mut-16* backgrounds. We found that *eri-6/7* transcript levels are strongly reduced ($\log_2$(fold change) ≤ -2) in the *prg-1; hrde-1* mutants, *mut-16* mutants, *sosi-1*Δ *mut-16* mutants, and *eri-6[e–f]*Δ *mut-16* mutants, further supporting that a loss of *sosi-1* and *eri-6[e–f]* siRNAs in the *mut-16 and prg-1; hrde-1* mutants causes a reduced expression of the *eri-6/7* transcript and that a loss of either the *sosi-1* or *eri-6[e–f]* locus alone is not sufficient to rescue *eri-6/7* expression (Figure 4F). We also found that the *sosi-1*Δ, *eri-6[e–f]*Δ, and *sosi-1 eri-6[e–f]*Δ mutants exhibited modestly reduced levels of *eri-6/7* transcripts compared to those of wild-type animals ($\log_2$(fold change) ≥ -1.5) (Figure 4F); however, this reduction in *eri-6/7* expression is not sufficient to affect the function of ERI-6/7 (Figures 4A–4E). In the *sosi-1 eri-6[e–f]*Δ *mut-16* mutants, which lack both *sosi-1* and *eri-6[e–f]* regions, the expression levels of *eri-6/7* were restored nearly to the level of wild-type animals (Figure 4F). Taken together, these data demonstrate that MUT-16 and the *mutator* complex are required for the production of HRDE-1-loaded 22G-RNAs that target the *eri-6[e–f]* and *sosi-1* regions, which, in turn, regulate the expression of the *eri-6/7* coding transcript and ultimately the production of ERGO-1-class 26G-RNAs. The reduction in ERGO-1-class 26G-RNAs in the *sosi-1*Δ *mut-16* and *eri-6[e–f]*Δ *mut-16* mutants indicates that mRNA expression from either *eri-6[e–f]* or *sosi-1* is sufficient to disrupt the expression of the *eri-6* and *eri-7* coding regions and production of the ERI-6/7 protein.

Modulation of the ERGO-1 26G-RNA Pathway Leads to Fine Tuning of the Production of MUT-16-Dependent 22G-RNA Classes

Previously, it was proposed that ERI proteins inhibit the exogenous RNAi pathway by competing for factors shared between the ERGO-1-class 26G-RNA pathway and the exogenous RNAi pathway (Duchaine et al., 2006; Lee et al., 2006). ERI-6/7 is required exclusively for the production of 26G-RNAs bound by the Argonaute ERGO-1, and both *eri-6/7* and *ergo-1* mutants exhibit an enhanced RNAi (Eri) phenotype (Fischer et al., 2008; Yigit et al., 2006). If mRNAs targeted by ERGO-1-class 26G-RNAs compete with mRNAs targeted by other primary siRNA pathways for siRNA amplification by the *mutator* complex, depletion of ERGO-1-class 26G-RNAs could lead to an increased production of other classes of endogenous *mutator*-dependent 22G-RNAs (Figure 5A). Based on our observation that MUT-16-dependent 22G-RNAs targeting the *sosi-1* and *eri-6[e–f]* regions is required for proper ERI-6/7 function, we hypothesized that these regions act as sensors for the production of non-ERGO-1-class 22G-RNAs and modulate expression of *eri-6/7* to maintain homeostasis and proper functioning of the exogenous and endogenous RNAi pathways. To determine whether we could observe changes in *mutator*-dependent small RNA populations as a result of a loss of ERGO-1-class 26G-RNAs, we assessed changes in the *mutator*-dependent small RNA classes in *ergo-1* mutants compared to wild-type animals. As expected, we found that loci annotated as ERGO-1 targets had significantly reduced levels of mapping small RNAs compared to miRNAs, which are not amplified by the *mutator* complex (Figure 5B). In contrast, we found that annotated piRNA target genes, *mutator* target genes, and RDE-1 target genes had significantly increased levels of corresponding small RNAs compared to miRNAs (Figure 5B). It should be noted that levels of small RNAs mapping to miRNAs in *ergo-1* mutants appear reduced compared to those in wild-type animals; however, because this analysis depends on normalizing to total library depth, an increase in the production of many MUT-16-dependent 22G-RNAs could result in an apparent decrease in other classes of small RNAs, including miRNAs. As an alternative analysis, we performed an enrichment analysis on genes with increased levels of small RNAs in *ergo-1* mutants compared to wild-type animals. We found that genes with significantly increased levels of mapped small RNAs in *ergo-1* mutants were enriched for piRNA targets, *mutator* targets, and RDE-1 targets and depleted for ERGO-1 target genes. CSR-1 target genes, whose 22G-RNAs are not amplified by the *mutator* complex, were neither significantly enriched nor significantly depleted (Figure 5C). These bioinformatic analyses confirm that when ERGO-1-class 26G-RNAs, and their downstream 22G-RNAs, are depleted, there is a corresponding increase in the other major classes of MUT-16-dependent small RNAs.

Taken together, our results reveal a regulatory feedback mechanism contained within the small RNA pathway in which the levels of ERGO-1 class 26G-RNAs and their downstream 22G-RNAs can be modulated to allow for increased production of other MUT-16-dependent 22G-RNA classes by HRDE-1-loaded 22G-RNAs, which ultimately may help maintain the robustness of the RNAi pathways.

DISCUSSION

Typically, when a locus is regulated by a small RNA pathway, its transcript is directly targeted by complementary Argonaute-loaded small RNAs that conduct transcriptional or post-transcriptional silencing of the target locus (Buckley et al., 2012; Burkhart et al., 2011; Claycomb, 2014; Gu et al., 2012; Guang et al., 2008, 2010; Hutvagner and Simard, 2008). Here, we show that HRDE-1-loaded 22G-RNAs targeting the regions of *sosi-1* and *eri-6[e–f]* downregulate *sosi-1* and *eri-6[e–f]*, which

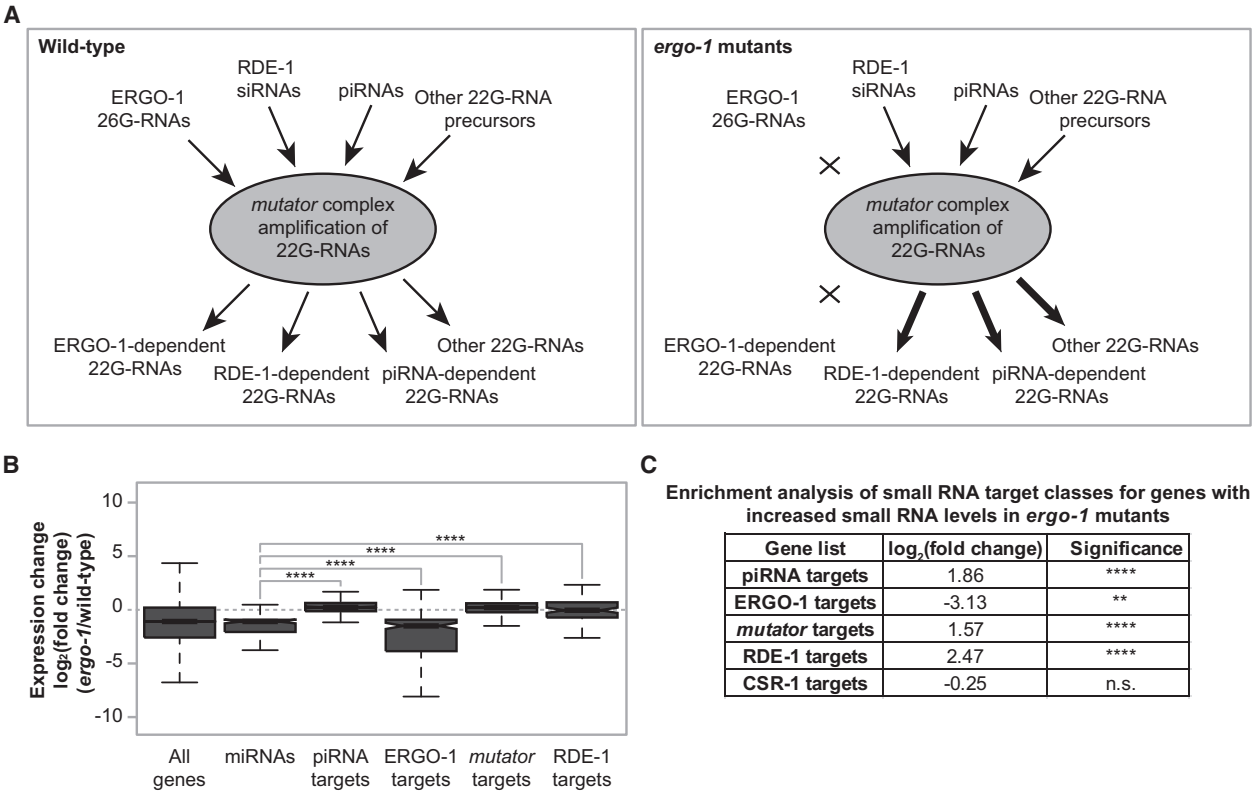

Enrichment analysis of small RNA target classes for genes with increased small RNA levels in *ergo-1* mutants

Gene list	log_2(fold change)	Significance
piRNA targets	1.86	****
ERGO-1 targets	-3.13	**
***mutator* targets**	1.57	****
RDE-1 targets	2.47	****
CSR-1 targets	-0.25	n.s.

Figure 5. Modulation of ERGO-1-Class 26G-RNAs Leads to Fine Tuning of the Production of MUT-16-Dependent 22G-RNA Classes

(A) Schema of competition for resources during amplification of MUT-16-dependent 22G-RNA classes.

(B) Comparison of total small RNA levels in wild-type animals compared to *ergo-1* mutants for known small RNA pathway targets. Notches indicate the 95% confidence interval of the median; black line indicates median. Significance between the log_2(fold change) for miRNAs compared to each class is indicated.

(C) Enrichment analysis for piRNA target genes, ERGO-1 target genes, *mutator* target genes, RDE-1 target genes, and CSR-1 target genes among the genes with increased mapped small RNAs in *ergo-1* mutants. **$p \leq 0.01$; **** $p \leq 0.0001$.

ultimately promotes the expression of the *trans*-spliced *eri-6/7* mRNA. The loss of the *sosi-1* region, the *eri-6[e–f]* region, or both regions does not affect ERI-6/7 function in wild-type animals. Furthermore, deletion of both regions eliminates the dependency of the *eri-6/7 trans*-spliced transcript on *mut-16* expression. These results indicate that, in *mut-16* mutants, the loss of 22G-RNAs targeting the *sosi-1* and *eri-6[e–f]* regions, and subsequent reduced expression of *trans*-spliced *eri-6/7*, is the underlying cause of the failure to produce ERGO-1-class 26G-RNAs. This small-RNA-mediated feedback loop explains the long-standing question of why *mut-16* mutants are defective in the synthesis of ERGO-1-class 26G-RNAs, which are produced upstream of MUT-16 in the small RNA pathway. Furthermore, when ERGO-1 class 26G-RNAs are lost, we observe increased levels of 22G-RNAs at other MUT-16-dependent loci (piRNA targets, *mutator* targets, and RDE-1 targets). Because the machinery for the production of other *mutator*-dependent 22G-RNAs seems to be a limiting resource (Duchaine et al., 2006; Lee et al., 2006), we propose that the 22G-RNAs targeting *sosi-1* and *eri-6[e–f]*, within the *eri-6/7* locus, may act as a sensor for functioning of the *mutator* 22G-RNA biogenesis pathway. Thus, when small RNA levels at *sosi-1* and *eri-6[e–f]* regions are reduced, this change allows for reallocation of resources away from the ERGO-1 class 26G-RNA pathway and toward the exogenous RNAi, piRNA, and other small RNA pathways more critical for fertility and maintaining appropriate germline gene expression (Figure 6A).

Furthermore, it was previously reported that *hrde-1* mutants, which cannot perform germline nuclear RNAi and therefore fail to promote H3K9me3 deposition at RNAi target loci, exhibited a 50% reduction in *eri-6/7* expression (Ni et al., 2014). Based on our discovery of 22G-RNA sensors nested within the *eri-6* genomic locus, we propose that the reduction of *eri-6/7* expression in *hrde-1* mutants is a direct result of this feedback mechanism. De-repression of *sosi-1*, and the resulting significant reduction of the *eri-6/7* mRNA, can occur whether there is a loss of secondary siRNAs or loss of H3K9me3 deposition by the germline nuclear RNAi pathway targeting the locus.

Biological circuits use feedback mechanisms to provide homeostatic regulation by maintaining appropriate levels of proteins. A recent study in *Drosophila melanogaster* that focused on the SUMO ligase Su(var)2-10, which links the piRNA-loaded Piwi complex to the silencing effector complex that induces H3K9me3 deposition at target loci, identified an autoregulatory

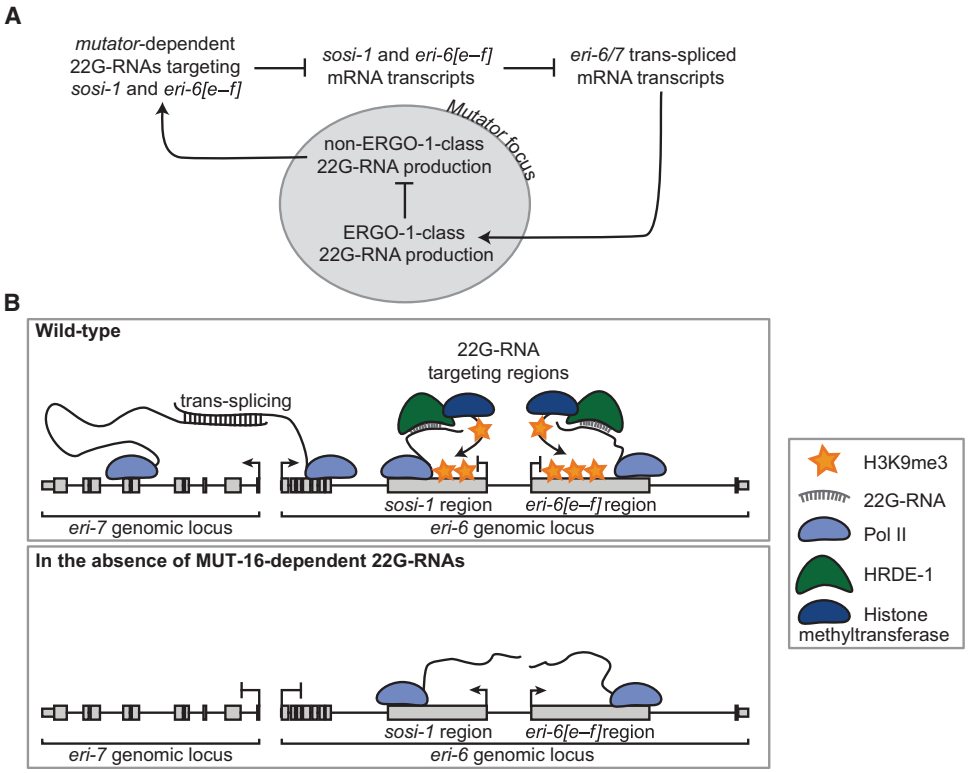

Figure 6. A Small-RNA-Mediated Feedback Mechanism Regulates the Production of Distinct 22G-RNA Classes
(A and B) Model of the feedback loop regulating *eri-6/7* expression and function through sensing of MUT-16-dependent 22G-RNAs.

feedback loop in which several factors involved in heterochromatin formation and maintenance were marked by H3K9me3 in a Su(var)2-10-dependent manner to maintain the proper ratio and boundaries of heterochromatin versus euchromatin (Ninova et al., 2020). In addition, the loss of Su(var)2-10-dependent H3K9me3 at target gene loci resulted in spurious differential expression of isoforms or internal genes (Ninova et al., 2020), similar to the spurious expression of *sosi-1* and *eri-6[e–f]* we observed in *mut-16* mutants. In yeast, a similar feedback mechanism was identified in which the H3K9 methyltransferase *clr4* is suppressed by H3K9me3 to ensure there is not inappropriate spreading of heterochromatin (Wang et al., 2015). Our work revealed a small-RNA-mediated feedback mechanism in which a factor involved in the RNAi pathways contains a sensor repressed by H3K9me3 deposition guided by 22G-RNAs. Future studies to determine the existence of other such feedback mechanisms in the evolutionarily conserved small RNA pathways will provide invaluable insights into how these regulatory mechanisms maintain homeostatic regulation in order to maintain proper levels of each class of siRNAs.

STAR★METHODS

Detailed methods are provided in the online version of this paper and include the following:

- KEY RESOURCES TABLE
- RESOURCE AVAILABILITY
  - Lead Contact
  - Materials Availability
  - Data and Code Availability
- EXPERIMENTAL MODEL AND SUBJECT DETAILS
  - *C. elegans* Strains
- METHOD DETAILS
  - Strain Construction
  - RNAi Assay
  - RNA Extraction
  - cDNA Preparation and qPCR Reactions
  - Small RNA Library Preparation
  - mRNA-seq library preparation
- QUANTIFICATION AND STATISTICAL ANALYSIS
  - Bioinformatic Analysis of mRNA-seq and Small RNA-seq Libraries
  - Statistical Analysis of qPCR Reactions

SUPPLEMENTAL INFORMATION

Supplemental Information can be found online at https://doi.org/10.1016/j.celrep.2020.108279.

ACKNOWLEDGMENTS

We thank the members of the Phillips lab for helpful discussions and feedback on the manuscript. Some strains were provided by the CGC, which is funded by NIH Office of Research Infrastructure Programs (P40 OD010440).

Next-generation sequencing was performed by the USC Molecular Genomics Core, which is supported by award number P30 CA014089 from the National Cancer Institute. This work was supported in part by a Basil O'Connor Starter Scholar Research Award from the March of Dimes Foundation grant no. 5-FY17-38 (to C.M.P.) and the National Institutes of Health grant R35 GM119656 (to C.M.P.). C.M.P. is a Pew Scholar in the Biomedical Sciences supported by the Pew Charitable Trusts. The funders had no role in study design, data collection and analysis, decision to publish, or preparation of the manuscript.

AUTHOR CONTRIBUTIONS

Conceptualization, A.K.R. and C.M.P.; Investigation, A.K.R.; Formal Analysis, A.K.R.; Writing – Original Draft, A.K.R.; Writing – Review & Editing, A.K.R. and C.M.P.; Visualization, A.K.R.; Funding Acquisition, C.M.P.; Supervision, C.M.P.

DECLARATION OF INTERESTS

The authors declare no competing interests.

Received: March 12, 2020
Revised: August 27, 2020
Accepted: September 24, 2020
Published: October 20, 2020

REFERENCES

Arribere, J.A., Bell, R.T., Fu, B.X., Artiles, K.L., Hartman, P.S., and Fire, A.Z. (2014). Efficient marker-free recovery of custom genetic modifications with CRISPR/Cas9 in Caenorhabditis elegans. Genetics *198*, 837–846.

Ashe, A., Sapetschnig, A., Weick, E.M., Mitchell, J., Bagijn, M.P., Cording, A.C., Doebley, A.L., Goldstein, L.D., Lehrbach, N.J., Le Pen, J., et al. (2012). piRNAs can trigger a multigenerational epigenetic memory in the germline of C. elegans. Cell *150*, 88–99.

Bernstein, E., Caudy, A.A., Hammond, S.M., and Hannon, G.J. (2001). Role for a bidentate ribonuclease in the initiation step of RNA interference. Nature *409*, 363–366.

Bosher, J.M., Dufourcq, P., Sookhareea, S., and Labouesse, M. (1999). RNA interference can target pre-mRNA: consequences for gene expression in a Caenorhabditis elegans operon. Genetics *153*, 1245–1256.

Brenner, S. (1974). The genetics of Caenorhabditis elegans. Genetics *77*, 71–94.

Buckley, B.A., Burkhart, K.B., Gu, S.G., Spracklin, G., Kershner, A., Fritz, H., Kimble, J., Fire, A., and Kennedy, S. (2012). A nuclear Argonaute promotes multigenerational epigenetic inheritance and germline immortality. Nature *489*, 447–451.

Burkhart, K.B., Guang, S., Buckley, B.A., Wong, L., Bochner, A.F., and Kennedy, S. (2011). A pre-mRNA-associating factor links endogenous siRNAs to chromatin regulation. PLoS Genet. *7*, e1002249.

Castel, S.E., and Martienssen, R.A. (2013). RNA interference in the nucleus: roles for small RNAs in transcription, epigenetics and beyond. Nat. Rev. Genet. *14*, 100–112.

Claycomb, J.M. (2014). Ancient endo-siRNA pathways reveal new tricks. Curr. Biol. *24*, R703–R715.

Dokshin, G.A., Ghanta, K.S., Piscopo, K.M., and Mello, C.C. (2018). Robust Genome Editing with Short Single-Stranded and Long, Partially Single-Stranded DNA Donors in *Caenorhabditis elegans*. Genetics *210*, 781–787.

Duchaine, T.F., Wohlschlegel, J.A., Kennedy, S., Bei, Y., Conte, D., Jr., Pang, K., Brownell, D.R., Harding, S., Mitani, S., Ruvkun, G., et al. (2006). Functional proteomics reveals the biochemical niche of C. elegans DCR-1 in multiple small-RNA-mediated pathways. Cell *124*, 343–354.

Fischer, S.E., Butler, M.D., Pan, Q., and Ruvkun, G. (2008). Trans-splicing in C. elegans generates the negative RNAi regulator ERI-6/7. Nature *455*, 491–496.

Fischer, S.E., Montgomery, T.A., Zhang, C., Fahlgren, N., Breen, P.C., Hwang, A., Sullivan, C.M., Carrington, J.C., and Ruvkun, G. (2011). The ERI-6/7 helicase acts at the first stage of an siRNA amplification pathway that targets recent gene duplications. PLoS Genet. *7*, e1002369.

Gent, J.I., Lamm, A.T., Pavelec, D.M., Maniar, J.M., Parameswaran, P., Tao, L., Kennedy, S., and Fire, A.Z. (2010). Distinct phases of siRNA synthesis in an endogenous RNAi pathway in C. elegans soma. Mol. Cell *37*, 679–689.

Ghildiyal, M., and Zamore, P.D. (2009). Small silencing RNAs: an expanding universe. Nat. Rev. Genet. *10*, 94–108.

Gu, W., Shirayama, M., Conte, D., Jr., Vasale, J., Batista, P.J., Claycomb, J.M., Moresco, J.J., Youngman, E.M., Keys, J., Stoltz, M.J., et al. (2009). Distinct argonaute-mediated 22G-RNA pathways direct genome surveillance in the C. elegans germline. Mol. Cell *36*, 231–244.

Gu, S.G., Pak, J., Guang, S., Maniar, J.M., Kennedy, S., and Fire, A. (2012). Amplification of siRNA in Caenorhabditis elegans generates a transgenerational sequence-targeted histone H3 lysine 9 methylation footprint. Nat. Genet. *44*, 157–164.

Guang, S., Bochner, A.F., Pavelec, D.M., Burkhart, K.B., Harding, S., Lachowiec, J., and Kennedy, S. (2008). An Argonaute transports siRNAs from the cytoplasm to the nucleus. Science *321*, 537–541.

Guang, S., Bochner, A.F., Burkhart, K.B., Burton, N., Pavelec, D.M., and Kennedy, S. (2010). Small regulatory RNAs inhibit RNA polymerase II during the elongation phase of transcription. Nature *465*, 1097–1101.

Hutvagner, G., and Simard, M.J. (2008). Argonaute proteins: key players in RNA silencing. Nat. Rev. Mol. Cell Biol. *9*, 22–32.

Kennedy, S., Wang, D., and Ruvkun, G. (2004). A conserved siRNA-degrading RNase negatively regulates RNA interference in C. elegans. Nature *427*, 645–649.

Ketting, R.F. (2011). The many faces of RNAi. Dev. Cell *20*, 148–161.

Ketting, R.F., Fischer, S.E., Bernstein, E., Sijen, T., Hannon, G.J., and Plasterk, R.H. (2001). Dicer functions in RNA interference and in synthesis of small RNA involved in developmental timing in C. elegans. Genes Dev. *15*, 2654–2659.

Kim, D., Langmead, B., and Salzberg, S.L. (2015). HISAT: a fast spliced aligner with low memory requirements. Nat. Methods *12*, 357–360.

Langmead, B., and Salzberg, S.L. (2012). Fast gapped-read alignment with Bowtie 2. Nat. Methods *9*, 357–359.

Lee, S.R., and Collins, K. (2007). Physical and functional coupling of RNA-dependent RNA polymerase and Dicer in the biogenesis of endogenous siRNAs. Nat. Struct. Mol. Biol. *14*, 604–610.

Lee, R.C., Hammell, C.M., and Ambros, V. (2006). Interacting endogenous and exogenous RNAi pathways in Caenorhabditis elegans. RNA *12*, 589–597.

Lee, H.C., Gu, W., Shirayama, M., Youngman, E., Conte, D., Jr., and Mello, C.C. (2012). C. elegans piRNAs mediate the genome-wide surveillance of germline transcripts. Cell *150*, 78–87.

Li, H., Handsaker, B., Wysoker, A., Fennell, T., Ruan, J., Homer, N., Marth, G., Abecasis, G., and Durbin, R.; 1000 Genome Project Data Processing Subgroup (2009). The Sequence Alignment/Map format and SAMtools. Bioinformatics *25*, 2078–2079.

Luteijn, M.J., van Bergeijk, P., Kaaij, L.J., Almeida, M.V., Roovers, E.F., Berezikov, E., and Ketting, R.F. (2012). Extremely stable Piwi-induced gene silencing in Caenorhabditis elegans. EMBO J. *31*, 3422–3430.

Martin, M. (2011). Cutadapt removes adapter sequences from high-throughput sequencing reads. EMBnet J *17*, 3.

Montgomery, T.A., Rim, Y.S., Zhang, C., Dowen, R.H., Phillips, C.M., Fischer, S.E., and Ruvkun, G. (2012). PIWI associated siRNAs and piRNAs specifically require the Caenorhabditis elegans HEN1 ortholog henn-1. PLoS Genet. *8*, e1002616.

Ni, J.Z., Chen, E., and Gu, S.G. (2014). Complex coding of endogenous siRNA, transcriptional silencing and H3K9 methylation on native targets of germline nuclear RNAi in C. elegans. BMC Genomics *15*, 1157.

Ninova, M., Godneeva, B., Chen, Y.A., Luo, Y., Prakash, S.J., Jankovics, F., Erdélyi, M., Aravin, A.A., and Fejes Tóth, K. (2020). The SUMO Ligase

Su(var)2-10 Controls Hetero- and Euchromatic Gene Expression via Establishing H3K9 Trimethylation and Negative Feedback Regulation. Mol. Cell *77*, 571–585.e4.

Paix, A., Folkmann, A., Rasoloson, D., and Seydoux, G. (2015). High Efficiency, Homology-Directed Genome Editing in Caenorhabditis elegans Using CRISPR-Cas9 Ribonucleoprotein Complexes. Genetics *201*, 47–54.

Pak, J., and Fire, A. (2007). Distinct populations of primary and secondary effectors during RNAi in C. elegans. Science *315*, 241–244.

Patro, R., Duggal, G., Love, M.I., Irizarry, R.A., and Kingsford, C. (2017). Salmon provides fast and bias-aware quantification of transcript expression. Nat. Methods *14*, 417–419.

Phillips, C.M., Montgomery, T.A., Breen, P.C., and Ruvkun, G. (2012). MUT-16 promotes formation of perinuclear mutator foci required for RNA silencing in the C. elegans germline. Genes Dev. *26*, 1433–1444.

Phillips, C.M., Montgomery, B.E., Breen, P.C., Roovers, E.F., Rim, Y.S., Ohsumi, T.K., Newman, M.A., van Wolfswinkel, J.C., Ketting, R.F., Ruvkun, G., and Montgomery, T.A. (2014). MUT-14 and SMUT-1 DEAD box RNA helicases have overlapping roles in germline RNAi and endogenous siRNA formation. Curr. Biol. *24*, 839–844.

Robinson, J.T., Thorvaldsdóttir, H., Winckler, W., Guttman, M., Lander, E.S., Getz, G., and Mesirov, J.P. (2011). Integrative genomics viewer. Nat. Biotechnol. *29*, 24–26.

Rogers, A.K., and Phillips, C.M. (2020). RNAi pathways repress reprogramming of C. elegans germ cells during heat stress. Nucleic Acids Res. *48*, 4256–4273.

Shen, E.Z., Chen, H., Ozturk, A.R., Tu, S., Shirayama, M., Tang, W., Ding, Y.H., Dai, S.Y., Weng, Z., and Mello, C.C. (2018). Identification of piRNA Binding Sites Reveals the Argonaute Regulatory Landscape of the C. elegans Germline. Cell *172*, 937–951.e18.

Shirayama, M., Seth, M., Lee, H.C., Gu, W., Ishidate, T., Conte, D., Jr., and Mello, C.C. (2012). piRNAs initiate an epigenetic memory of nonself RNA in the C. elegans germline. Cell *150*, 65–77.

Sijen, T., Steiner, F.A., Thijssen, K.L., and Plasterk, R.H. (2007). Secondary siRNAs result from unprimed RNA synthesis and form a distinct class. Science *315*, 244–247.

Svendsen, J.M., Reed, K.J., Vijayasarathy, T., Montgomery, B.E., Tucci, R.M., Brown, K.C., Marks, T.N., Nguyen, D.A.H., Phillips, C.M., and Montgomery, T.A. (2019). henn-1/HEN1 Promotes Germline Immortality in Caenorhabditis elegans. Cell Rep. *29*, 3187–3199.e4.

Tsai, H.Y., Chen, C.C., Conte, D., Jr., Moresco, J.J., Chaves, D.A., Mitani, S., Yates, J.R., 3rd, Tsai, M.D., and Mello, C.C. (2015). A ribonuclease coordinates siRNA amplification and mRNA cleavage during RNAi. Cell *160*, 407–419.

Vasale, J.J., Gu, W., Thivierge, C., Batista, P.J., Claycomb, J.M., Youngman, E.M., Duchaine, T.F., Mello, C.C., and Conte, D., Jr. (2010). Sequential rounds of RNA-dependent RNA transcription drive endogenous small-RNA biogenesis in the ERGO-1/Argonaute pathway. Proc. Natl. Acad. Sci. USA *107*, 3582–3587.

Wang, J., Reddy, B.D., and Jia, S. (2015). Rapid epigenetic adaptation to uncontrolled heterochromatin spreading. Elife *4*, e06179.

Wu, W.S., Brown, J.S., Chen, T.T., Chu, Y.H., Huang, W.C., Tu, S., and Lee, H.C. (2019). piRTarBase: a database of piRNA targeting sites and their roles in gene regulation. Nucleic Acids Res. *47*, D181–D187.

Yigit, E., Batista, P.J., Bei, Y., Pang, K.M., Chen, C.C., Tolia, N.H., Joshua-Tor, L., Mitani, S., Simard, M.J., and Mello, C.C. (2006). Analysis of the C. elegans Argonaute family reveals that distinct Argonautes act sequentially during RNAi. Cell *127*, 747–757.

Zhang, C., Montgomery, T.A., Gabel, H.W., Fischer, S.E., Phillips, C.M., Fahlgren, N., Sullivan, C.M., Carrington, J.C., and Ruvkun, G. (2011). mut-16 and other mutator class genes modulate 22G and 26G siRNA pathways in Caenorhabditis elegans. Proc. Natl. Acad. Sci. USA *108*, 1201–1208.

Zhang, D., Tu, S., Stubna, M., Wu, W.S., Huang, W.C., Weng, Z., and Lee, H.C. (2018). The piRNA targeting rules and the resistance to piRNA silencing in endogenous genes. Science *359*, 587–592.

Zhuang, J.J., Banse, S.A., and Hunter, C.P. (2013). The nuclear argonaute NRDE-3 contributes to transitive RNAi in Caenorhabditis elegans. Genetics *194*, 117–131.

STAR★METHODS

KEY RESOURCES TABLE

REAGENT or RESOURCE	SOURCE	IDENTIFIER
Chemicals, Peptides, and Recombinant Proteins		
TRIzol Reagent	Life Technologies	Cat# 15596026
RNaseOUT	ThermoFisher Scientific	Cat# 10777019
TURBO DNase	ThermoFisher Scientific	Cat# AM2238
SuperScript III Reverse Transcriptase	ThermoFisher Scientific	Cat# 18080093
2x iTaq Universal SYBER Green Supermix	Biorad	Cat# 1725121
Multiscribe Reverse Transcriptase	ThermoFisher Scientific	Cat# 4311235
2x TaqMan Fast Advanced Master Mix	ThermoFisher Scientific	Cat# 4444557
Alt-R S.p. Cas9 Nuclease V3	Integrated DNA Technologies	Cat# 1081058
Critical Commercial Assays		
Qubit 1X dsDNA HS Assay Kit	ThermoFisher Scientific	Cat# Q33230
Dynabeads mRNA Purification Kit	ThermoFisher Scientific	Cat# 61006
NEBNext Ultra II Directional RNA Library Prep Kit for Illumina	New England Biolabs	Cat# E7760S
NEBNext multiplex oligos for Illumina	New England Biolabs	Cat# E7335S
Deposited Data		
Raw and analyzed data	This paper.	GEO: GSE145217
Raw and analyzed data for wild-type and *mut-16* mutant small RNA-seq and mRNA-seq	Rogers and Phillips, 2020	GEO: GSE134573
Experimental Models: Organisms/Strains		
C. elegans: Strain N2 (wild-type)	Caenorhabditis Genetics Center	RRID:WB-STRAIN:N2_(ancestral)
C. elegans: Strain NL1810 – *mut-16(pk710) I.*	Caenorhabditis Genetics Center	RRID:WB-STRAIN:NL1810; Wormbase: WBVar00239329(pk710)
C. elegans: Strain WM158 – *ergo-1(tm1860) V.*	Caenorhabditis Genetics Center	RRID:WB-STRAIN:WBStrain00040450
C. elegans: Strain SX922 – *prg-1(n4357) I.*	Caenorhabditis Genetics Center	RRID:WB-STRAIN:WBStrain00034642
C. elegans: Strain USC1332 – *eri-6[e-f]Δ(cmp261) I.*	The Phillips Laboratory	USC1332
C. elegans: Strain USC1333 – *eri-6[e-f]Δ(cmp261) mut-16(pk710) I.*	The Phillips Laboratory	USC1333
C. elegans: Strain USC1335 – *sosi-1Δ(cmp262) I.*	The Phillips Laboratory	USC1335
C. elegans: Strain USC1337 – *sosi-1Δ(cmp262) mut-16(pk710) I.*	The Phillips Laboratory	USC1337
C. elegans: Strain USC1338 – *sosi-1Δ eri-6[e-f]Δ(cmp263) I.*	The Phillips Laboratory	USC1338
C. elegans: Strain USC1355 – *sosi-1 eri-6[e-f]Δ(cmp263) mut-16(pk710) I.*	The Phillips Laboratory	USC1355
C. elegans: Strain USC1387 – *prg-1(n4357) I; hrde-1(tm1200) III.*	The Phillips Laboratory	USC1387
C. elegans: Strain USC1388 – *prg-1(n4357) I; ergo-1(tm1860) V.*	The Phillips Laboratory	USC1388
Oligonucleotides		
Primers used for experiments, See Table S1.	This paper.	N/A
Software and Algorithms		
Cutadapt	Martin, 2011	https://cutadapt.readthedocs.io/en/stable/
HISAT2	Kim et al., 2015	https://ccb.jhu.edu/software/hisat2/index.shtml
Salmon	Patro et al., 2017	https://combine-lab.github.io/salmon/
Bowtie2	Langmead and Salzberg, 2012	http://bowtie-bio.sourceforge.net/bowtie2/index.shtml

(*Continued on next page*)

Continued

REAGENT or RESOURCE	SOURCE	IDENTIFIER
Samtools	Li et al., 2009	http://samtools.sourceforge.net/
Integrative Genomics Viewer 2.3.68	Robinson et al., 2011	https://software.broadinstitute.org/software/igv/
Other		
15% Criterion TBE-Urea Polyacrylamide Gel, 12+2 well	Criterion	Cat# 3450091
4–12% Bis-Tris polyacrylamide Gels	ThermoFisher Scientific	Cat# NP0322BOX

RESOURCE AVAILABILITY

Lead Contact

Further information and requests for resources and reagents should be directed to, and will be fulfilled by the Lead Contact, Carolyn M. Phillips (cphil@usc.edu).

Materials Availability

C. elegans strains generated in this study are deposited and maintained in the Phillips Lab strain collection (USC1332 – *eri-6[e–f]Δ(cmp261) I,* USC1333 – *eri-6[e–f]Δ(cmp261) mut-16(pk710) I,* USC1335 – *sosi-1Δ(cmp262) I,* USC1337 – *sosi-1Δ(cmp262) mut-16(pk710) I,* USC1338 – *sosi-1Δ eri-6[e–f]Δ(cmp263) I,* USC1355 – *sosi-1 eri-6[e–f]Δ(cmp263) mut-16(pk710) I*, USC1387 – *prg-1(n4357) I; hrde-1(tm1200) III*, and USC1388 – *prg-1(n4357); ergo-1(tm1860) V)*.

Data and Code Availability

The accession number for the de-multiplexed raw sequencing data, in fastq format, for *prg-1, ergo-1, eri-6[e–f]Δ, eri-6[e–f]Δ mut-16, sosi-1Δ, sosi-1Δ mut-16, sosi-1 eri-6[e–f]Δ, sosi-1 eri-6[e–f]Δ mut-16, prg-1; hrde-1, and prg-1; ergo-1* mutants small RNA-seq and mRNA-seq libraries reported in this paper is NCBI's Gene Expression Omnibus GEO: GSE145217.

EXPERIMENTAL MODEL AND SUBJECT DETAILS

C. elegans Strains

Unless otherwise stated, synchronized hermaphroditic *C. elegans* worms were grown to adulthood at 20°C according to standard conditions (Brenner, 1974).

METHOD DETAILS

Strain Construction

For the generation of the *eri-6[e–f]* deletion mutant, the *sosi-1* deletion mutant, and the *sosi-1 eri-6[e–f]* double deletion mutant, CRISPR injections were performed according to published protocols using an oligo repair template and RNA guides (Table S1; Dokshin et al., 2018; Paix et al., 2015). The injection mixes included 0.25 μg/μl Cas9 protein (IDT), 100 ng/μl tracrRNA (IDT), 14 ng/μl *dpy-10* crRNA, 21 ng/μl each gene-specific crRNA, 110 ng/μl *dpy-10* repair template and 110 ng/μl gene-specific repair template, and were injected into the wild-type (N2) strain (Dokshin et al., 2018; Paix et al., 2015). Post-injection, F1 animals with the Roller (Rol) or Dumpy (Dpy) phenotypes were plated individually and their progeny were PCR genotyped for the presence of the *eri-6[e–f]*, *sosi-1*, or *sosi-1 eri-6[e–f]* deletion mutants (Arribere et al., 2014).

RNAi Assay

Feeding RNAi assays were done at 20°C. For L4440 (control), *dpy-13*, and *lir-1* RNAi, 120 synchronized L1s of each genotype were placed on *E. coli* expressing the dsRNA. P0 animals were scored after ~3 days on RNAi for the following phenotypes – *dpy-13* RNAi: - indicates no phenotype, + indicates a weak phenotype (slightly Dumpy), and +++ indicates a strong phenotype (severely Dumpy) and for *lir-1* RNAi: - indicates no phenotype and +++ indicates a strong phenotype (Lethal). Representative images of scored phenotypes are shown in Figure 4A. All images were taken with 5x zoom on a Nikon SMZ645 stereomicroscope using an iPhone camera.

RNA Extraction

Synchronized L1s of each strain were cultured for ~68hrs at 20°C and harvested as adults for RNA extraction. Worms were washed off plates using water and then settled on ice to form a pellet. For embryo RNA samples, embryos were extracted from adult animals by bleaching (14% bleach + 10% 5M NaOH) until adult animals degraded and embryos released, and then washed in water. Adults or embryos were resuspended in 1mL TRIzol reagent (Life Technologies) and freeze-thawed on dry ice followed by vortexing. Debris

was pelleted using centrifugation and the supernatant containing RNA was collected. 0.2 volume chloroform was added to the supernatant, vortexed, centrifuged, and then the aqueous phase was transferred to a new tube. Samples were precipitated using isopropanol and rehydrated in 50 μL nuclease-free H_2O.

cDNA Preparation and qPCR Reactions

Adult RNA samples were DNase treated using DNase I Amplification Grade (ThermoFisher 18068015) and reverse transcribed with SuperScript III Reverse Transcriptase (ThermoFisher 18080093), following manufacturer's protocols. All real time PCR reactions were performed using the 2x iTaq Universal SYBER Green Supermix (Biorad 1725121). Quantitative RT-PCR for small RNA (TaqMan, Life Technologies) levels in embryo RNA samples were done according to Life Technologies recommendations using the TaqMan MicroRNA Reverse Transcription kit (ThermoFisher 4366597). All real time TaqMan PCR reactions were performed using the 2x TaqMan Fast Advanced Master Mix (ThermoFisher 4444557). All qRT-PCR reactions were run in a CFX96 Touch Real-Time PCR System (Biorad 1855196). Primers and small RNA sequences used are listed in Table S1.

Small RNA Library Preparation

Small RNAs (18- to 30- nt) were size selected on denaturing 15% polyacrylamide gels (Criterion 3450091) from total RNA samples. Libraries were prepared as previously described (Montgomery et al., 2012). Library quality was assessed (Agilent BioAnalyzer Chip) and concentration was determined using the Qubit 1X dsDNA HS Assay kit. Libraries were sequenced on the Illumina NextSeq500 (SE 75-bp reads) platform. Three biological replicates were generated for *prg-1*, *ergo-1*, *eri-6[e–f]*Δ, *eri-6[e–f]*Δ *mut-16*, *sosi-1*Δ, *sosi-1*Δ *mut-16*, *sosi-1 eri-6[e–f]*Δ, *sosi-1 eri-6[e–f]*Δ *mut-16*, *prg-1; hrde-1*, and *prg-1; ergo-1* mutants.

mRNA-seq library preparation

Nuclease-free H_2O was added to 7.5 μg of each RNA sample, extracted from whole animals, to a final volume of 100 μL. Samples were incubated at 65°C for 2 minutes then incubated on ice. The Dynabeads mRNA Purification Kit (ThermoFisher 61006) was used according to the manufacturer's protocol. 20 μL of Dynabeads was used for each sample. 100ng of each mRNA sample was used to prepare libraries with the NEBNext Ultra II Directional RNA Library Prep Kit for Illumina (NEB E7760S) according to the manual, using NEBNext multiplex oligos for Illumina (NEB E7335S). Library quality was assessed (Agilent BioAnalyzer Chip) and concentration was determined using the Qubit 1X dsDNA HS Assay kit (ThermoFisher Q33231). Libraries were sequenced on the Illumina NextSeq500 (SE 75-bp reads) platform. Three biological replicates were generated for *eri-6[e–f]*Δ, *eri-6[e–f]*Δ *mut-16*, *sosi-1*Δ, *sosi-1*Δ *mut-16*, *sosi-1 eri-6[e–f]*Δ, *sosi-1 eri-6[e–f]*Δ *mut-16*, *prg-1; hrde-1*, and *prg-1; ergo-1* mutants.

QUANTIFICATION AND STATISTICAL ANALYSIS

Bioinformatic Analysis of mRNA-seq and Small RNA-seq Libraries

Sequences were parsed from adapters using Cutadapt (Martin, 2011) and mapped to the *C. elegans* genome, WS258, using HISAT2 and Bowtie2 (Langmead and Salzberg, 2012; Kim et al., 2015) and the transcriptome using Salmon (Patro et al., 2017). Data analysis was done using samtools (Li et al., 2009), R, Excel, and custom Python scripts. Reads per million were plotted along the WS258 genome using Integrative Genomics Viewer 2.3.68 (Robinson et al., 2011). ERGO-1 target genes were defined using our *ergo-1* libraries, and *mutator* target genes, piRNA target genes, RDE-1 target genes, and CSR-1 target genes were previously described (Gu et al., 2009; Lee et al., 2012; Phillips et al., 2014; Svendsen et al., 2019; Tsai et al., 2015; Zhang et al., 2011). Sequencing data is summarized in Table S2. For all sequencing experiments, n = 3 biological replicates for each condition examined. Statistical parameters, including $\log_2$(fold change), standard deviation, and statistical significance are reported in the figures.

Statistical Analysis of qPCR Reactions

For each qPCR experiment, n = 3 biological replicates, with 3 technical replicates, for each condition were examined. Statistical parameters, including $\log_2$(fold change), normalized as indicated, standard deviation, and statistical significance are reported in the figures.